Behavioral/Systems/Cognitive

High Sensitivity to Neuromodulator-Activated Signaling Pathways at Physiological [K^+] of Confocally Imaged Respiratory Center Neurons in On-Line-Calibrated Newborn Rat Brainstem Slices

Araya Ruangkittisakul,[1]* Stephan W. Schwarzacher,[2]* Lucia Secchia,[1] Betty Y. Poon,[1] Yonglie Ma,[1] Gregory D. Funk,[1]‡ and Klaus Ballanyi[1]‡

[1]Department of Physiology and Perinatal Research Centre, University of Alberta, Edmonton, Alberta, Canada T6G 2S2, and [2]Department of Clinical Neuroanatomy, University of Frankfurt, 60590 Frankfurt/Main, Germany

The pre-Bötzinger complex (PBC) inspiratory center remains active in a transverse brainstem slice. Such slices are studied at high (8–10 mM) superfusate [K^+], which could attenuate the sensitivity of the PBC to neuromodulators such as opiates. Findings may also be confounded because slice boundaries, drug injection sites, or location of rhythmogenic interneurons are rarely verified histologically. Thus, we first generated PBC slices with defined boundaries using novel "on-line histology" based on our finding that rostrocaudal extensions of brainstem respiratory marker nuclei are constant in newborn rats between postnatal days 0–4. At physiological superfusate [K^+] (3 mM), 500- and 600-μm-thick slices with the PBC in the center and the caudal boundary 0.70 and 0.76 mm caudal to the facial motonucleus generated rhythm for >2 and ~4 h, respectively. Rhythm was abolished by low nanomolar concentrations of the μ-opiate receptor agonist DAMGO ([D-Ala^2, *N*-Me-Phe^4, Gly^5-ol]enkephalin). After spontaneous arrest of bursting, rhythm was reactivated at clinically relevant or physiological concentrations by 3,5-dihydroxyphenylglycine, thyrotropin-releasing hormone, or rolipram, each affecting distinct second-messenger pathways. Two-photon/confocal Ca^{2+} imaging revealed that these agents reactivated the same PBC neurons initially active in 3 mM [K^+]. The data show that "calibrated" PBC slices at physiological [K^+] generate rhythm with a high sensitivity to neuromodulators for extended time periods, whereas spontaneous "*in vitro* apnea" is an important tool to study the interaction of signaling pathways that modulate rhythm. Our approaches and findings provide the basis for a pharmacological and structure–function analysis of the isolated respiratory center in a histologically well defined substrate at physiological [K^+].

Key words: **calcium imaging; confocal; brain stem; multiphoton; pre-Botzinger complex; respiratory rhythm**

Introduction

The pre-Bötzinger complex (PBC) constitutes a pivotal inspiratory center. Through microsection of newborn rat brainstems, it has been identified as a medullary region that extends between ~400 and 600 μm caudal to facial motonucleus and generates inspiratory rhythm in a transverse slice preparation (Smith et al., 1991). The hypothesized importance of the PBC for inspiratory rhythm generation has been confirmed in numerous studies combining electrophysiological PBC recording with microinjection of neuromodulators in both PBC slices and *in vivo* (Feldman et al., 2003; Feldman and Del Negro, 2006). Immunohistochemical studies have identified putative markers for PBC neurons such as μ-opiate and neurokinin-1-type substance P receptors (Gray et al., 1999). In turn, targeted lesioning of PBC neurons with substance P-tagged saporin profoundly perturbs breathing (Gray et al., 2001).

Despite agreement on the significance of the PBC slice model, it is recognized that the *in vitro* rhythm differs from respiratory activity *in vivo* (Richter and Spyer, 2001; Feldman and Del Negro, 2006). For example, low nanomolar concentrations of μ-opiate receptor agonists abolish inspiratory rhythm *in situ* (Manzke et al., 2003), whereas micromolar concentrations are typically necessary to abolish the slice rhythm (Johnson et al., 1994). Such discrepancies may reflect the routine use of superfusates with elevated (8–10 mM) [K^+] to study PBC slices. These high [K^+] levels may provide a powerful although nonspecific excitatory stimulus (Somjen, 2002) that may attenuate the sensitivity of the isolated PBC to neuromodulators. The original report on the PBC indicated that slices generate inspiratory activity in superfusate of physiological [K^+] (3 mM), but for brief periods only (Smith et al., 1991). Accordingly, it was a major aim of our study to examine the basic rhythm and responses to neuromodulators of PBC slices in physiological [K^+].

Received Aug. 3, 2006; revised Oct. 6, 2006; accepted Oct. 9, 2006.

This work was supported by the Canadian Institutes of Health Research (CIHR), the Alberta Heritage Foundation for Medical Research (AHFMR), the Canadian Foundation for Innovation, and the Alberta Innovation and Research Investments Program (Alberta Science and Research Authority). K.B. and G.D.F. are an AHFMR Scientist and a Senior Scholar, respectively. A.R. has been awarded a CIHR studentship (Maternal-Fetal-Newborn training grant).

*A.R. and S.W.S. contributed equally to this work.

‡G.D.F. and K.B. are coauthors.

Correspondence should be addressed to Klaus Ballanyi, Department of Physiology and Perinatal Research Centre, 220 HMRC, University of Alberta, Edmonton, Alberta, Canada T6G 2S2. E-mail: klaus.ballanyi@ualberta.ca.

DOI:10.1523/JNEUROSCI.3357-06.2006

 0270-6474/06/2611870-11$15.00/0

Furthermore, we exploited the fact that the rhythm would arrest after some time (Smith et al., 1991; Funk et al., 1993) and used this "*in vitro* apnea" as a tool to study reactivation of rhythm by neuromodulators affecting distinct second-messenger signaling pathways. Incorporation of two-photon/confocal Ca^{2+} imaging to simultaneously monitor the activity of multiple neurons (Yuste et al., 2006) allowed us to assess whether endogenous and evoked rhythms involve the same or distinct neuronal assemblies. The combined electrophysiological/imaging approach will establish network sensitivity to specific signaling cascades and may possibly reveal the potential involvement of particular neurotransmitter(s), before their putative washout from the slice, in maintaining network excitability or generating rhythm.

Critical to the success of these experiments was the generation of consistent PBC slices. For this, we developed "on-line histology" using a reference newborn rat brainstem atlas to generate slices with reproducible and defined rostrocaudal boundaries. The objective was to establish and analyze sustained inspiratory rhythm in "calibrated slices" containing the PBC in the middle. Our rationale was that failure of previous studies to obtain long-term rhythm in 3 mM $[K^+]$ might reflect slice topography. Specifically, slices with the PBC exposed to one boundary may lack subpopulation(s) of PBC neurons (or dendrites), such that connectivity and excitatory drive are reduced below levels required for rhythm.

Materials and Methods

Preparation and solutions. Experiments were performed on transverse brainstem slices from Sprague Dawley (SD) and Wistar (W) rats between postnatal day 0 (P0) and P4. Procedures were approved by the ethics committee of the University of Alberta. Animals were anesthetized with 2–3% isoflurane until the paw withdrawal reflex disappeared. They were then decerebrated and the neuraxis isolated at 18−20°C in saline containing the following (in mM): 120 NaCl, 3 KCl, 1 $CaCl_2$, 2 $MgSO_4$, 26 $NaHCO_3$, 1.25 NaH_2PO_4, and 20 D-glucose (pH adjusted to 7.4 by gassing with 95% O_2, 5% CO_2). After removal of the cerebellum and transverse sectioning at the pontomedullary junction and just rostral to the C_1 cervical segment, the brainstem was glued rostral side down to a metal plate. Serial transverse sections were made with a vibratome (Leica VT1000S; Leica Microsystems, Richmond Hill, Ontario, Canada) in caudal-to-rostral direction starting near the pyramidal decussation (Schwarzacher et al., 2002). Sectioning was stopped based on appearance of landmarks identified by on-line histology (see Results). One PBC-containing slice with rostrocaudal thickness of 500 or 600 μm was cut and fixed (caudal surface up) with insect pins on the silicone layer covering the bottom of the recording chamber (volume, 1.5 ml). Superfusate was administered at a flow rate of 5 ml/min via a peristaltic pump (Watson-Marlow Alitea-AB; Sin-Can, Calgary, Alberta, Canada). Superfusate temperature in the recording chamber was kept at 25−27°C (TC-324B; Harvard Apparatus, Saint-Laurent, Quebec, Canada).

Agents. Agents were as follows: [D-Ala^2, *N*-Me-Phe^4, Gly^5-ol]Enkephalin (DAMGO) (10–25 nM; stock 100 μM in superfusate), 3,5-dihydroxy-phenylglycine (DHPG) (0.1–10 μM; stock 10 mM in superfusate), thyrotropin-releasing hormone (TRH) (0.1–100 nM; stocks 1 μM and 1 mM in superfusate), rolipram (0.25, 1, and 5 μM; stocks 1 and 10 mM in dimethyl sulfoxide), theophylline (0.25 and 2.5 mM; added to superfusate), glutamate (1 mM; stock 1 M in superfusate), fluo-4 acetoxymethyl (fluo-4-AM) (0.5 mM; stock 5 mM in pluronic acid, 20% in dimethyl sulfoxide), agar–agar (6% in H_2O), fixation solution [4% paraformaldehyde in phosphate buffer (i.e., 1:2 mixture of 0.1 M NaH_2PO_4 plus 0.1 M Na_2HPO_4 in H_2O, pH 7.2)], and staining solution (1% thionin acetate in 0.1 M sodium acetate trihydrate plus 0.1 M acetic acid). Agents were obtained from Sigma (Oakville, Ontario, Canada) except salts for superfusate, sodium acetate trihydrate, acetic acid (Fisher Scientific, Ottawa, Ontario, Canada), DHPG (Tocris Biosciences, Ellisville, MO), theophylline, naloxone, glutamate (ICN Biomedicals, Costa Mesa, CA), and fluo-4-AM (TEF Labs, Austin, TX).

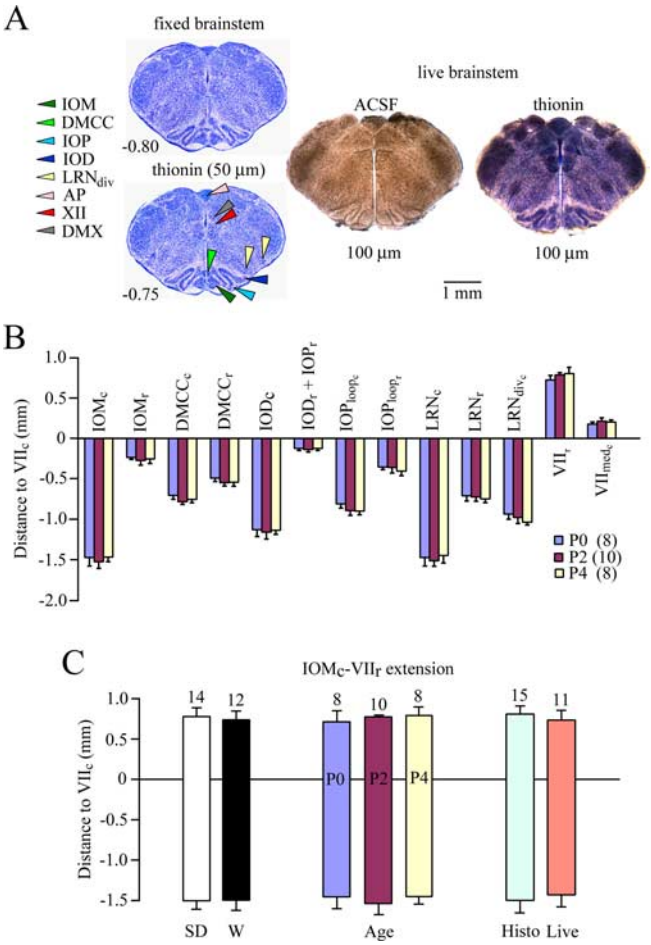

Figure 1. Constancy of rostrocaudal extensions of "respiratory marker nuclei" in the ventral brainstem of newborn SD and W rats between P0 and P4. ***A***, The left panel shows two serial, transverse sections (50 μm thin) of fixed, thionin-stained brainstem tissue from P2 W rat, which are part of a reference atlas (supplemental material, available at www.jneurosci.org). The middle panel shows a 100 μm section of living tissue taken at the rostrocaudal level encompassed by the two fixed sections in the left panel. The right panel is an image of the section in the middle panel taken after fixation and thionin staining. ***B***, Distances from the caudal end of VII motonucleus (VII$_c$) to the caudal (c) and rostral (r) boundaries of specific marker nuclei (negative value indicating location caudal to VII$_c$). ***C***, Location, relative to VII$_c$, of the boundaries of the most rostral (VII$_r$) and caudal (IOM$_c$) brainstem marker nuclei. Extensions are very similar when data are analyzed either from W versus SD rats, animals from both strains at different ages, or initially fixed (Histo) versus live preparations. The bars in ***B*** and ***C*** represent means ± SD; values above bars and in parentheses in ***B*** represent the number of preparations. The histology of some marker structures is shown in ***A***. Additional images of marker nuclei are in Figures 2*C* and 3 and the supplemental material (available at www.jneurosci.org). DMCC, Dorsomedial cell column of inferior olive (IO); IOM, medial IO; IOD, dorsal IO; IOP, principal IO; IOP$_{loop}$, lateral loop of IOP; LRN, lateral reticular nucleus; LRN$_{div}$, LRN divided in medial and lateral subnucleus; VII, facial motonucleus; VII$_{med}$, medial subnucleus of VII; AP, area postrema; XII, hypoglossal motonucleus; DMX, dorsal vagal motonucleus.

Electrophysiological recording. Discharge of ventral respiratory column (VRC) (Alheid et al., 2004) was recorded extracellularly with a differential amplifier (DAM 50; WPI, Sarasota, FL) via suction electrodes (outer diameter, 80–250 μm) filled with superfusate, positioned on the caudal slice surface. Signals were amplified (×10k), bandpass filtered (0.3–1 kHz), integrated, and recorded digitally (Powerlab/8SP; ADInstruments, Colorado Springs, CO).

Two-photon/confocal Ca^{2+} imaging. Rhythmic activity of newborn rat VRC neurons that express specific sets of voltage-activated Ca^{2+} channels (Onimaru et al., 1996, 2003) was visualized with imaging of cytosolic $[Ca^{2+}]$ (Yuste et al., 2006). The membrane-permeable Ca^{2+} sensitive dye fluo-4-AM (0.5 mM in superfusate) was backfilled into a broken

patch pipette (outer diameter, 5–10 μm) and pressure-injected (0.7–1.0 psi) for 10 min (Stosiek et al., 2003) into the VRC/PBC from the caudal surface while inspiratory activity was electrophysiologically monitored from the contralateral VRC/PBC. Fluorescence signals were measured using either a confocal microscope and software (20× XLUMPlanF1, numerical aperture, 0.95, objective; Olympus FV300; Carsen group, Markham, Ontario, Canada) or a FV300 connected with a Ti:Sa laser (10 W Mira/Verdi; Coherent, Santa Clara, CA) for two-photon imaging (Nikolenko et al., 2003). Within 10–20 min after injection, labeling revealed basic neuronal morphology and changes in fluorescence intensity that oscillated in phase with electrophysiological VRC/PBC activity. Stained areas were 200–300 μm in diameter. Ca^{2+} oscillations, cell bodies, and primary dendrites could be resolved at tissue depths up to 60 μm for confocal and 90 μm for 2-photon microscopy. Respiratory neurons were typically imaged at tissue depths between 30 and 60 μm. Rhythmic Ca^{2+} rises were visualized in up to 10 cells (typically 3–6) in a single *xy*-image plane. The stained region was monitored using a 2–3× digital zoom at reduced settings for *y*-axis scanning. Compared with full-frame acquisition (512 × 512 pixels), such "clipped mode" imaging sampled an area of 512 × 100–220 pixels and provided scan rates of 1.25–1.43 scans/s sufficient to detect 70–100% of peak respiratory Ca^{2+} rises. The morphology of cell bodies and primary dendrites was revealed by combining "*z*-stack" imaging (single *z*-steps, 0.5 μm) with three-dimensional (3D) animation using Fluoview software. Fluo-4 fluorescence emission is weak at low cytosolic [Ca^{2+}] (Stosiek et al., 2003; Yuste et al., 2006). Therefore, to improve morphological reconstruction, slices were exposed to glutamate (0.25–1 mM; 5–10 min) after the experiments and *z*-stack image series acquired. Glutamate-induced fluorescence signals were 3–10 times larger than those associated with spontaneous or drug-induced inspiratory activity.

Histological procedures. Respiratory marker nuclei were mapped in 50 and 100 μm serial brainstem sections. Brainstems and brainstem slices were kept for >1 h in fixation solution (see above, Agents). For staining, slices were incubated in phosphate buffer for 2 min and immersed for 45–60 s in thionin staining solution (see above, Agents). Slices were consecutively "washed" with 50% ethanol (2 min), 70% ethanol (1 min), 50% ethanol (2 min), and phosphate buffer (2 min). One hundred micrometer sections caudal and rostral to a prospective rhythmic slice were fixed for at least 15 min and stained for 30–40 s with the above solutions. Sections were transferred on a "hanging drop" glass slide (Fisher Scientific) to a microscope (Standard 16; magnification, 32×; Carl Zeiss, Jena, Germany) and photographed (PL-A642, 1.3 megapixel; PixeLINK, Ottawa, Ontario, Canada). PBC slices were stained after experiments using an identical method, except they were immersed in thionin for 90 s. Stained PBC slices were transferred in phosphate buffer to a Petri dish and photographed (PL-A686, 6.6 megapixel; PixeLINK) under a stereo microscope (Zeiss SR15; magnification, 32×).

Data analysis. Inspiratory activity of PBC slices in 3 mM [K^+] solution was continuously recorded at a sampling rate of 1 kHz. Burst rate was averaged every 20 min over 2 min time windows. "Longevity" of rhythm was defined as the time from start of recording until the time when the period between consecutive bursts exceeded 5 min. Burst duration was defined using ClampFit software (Molecular Devices, Chicago, IL) as the time interval from when the signal increased above and decreased below a threshold set at 10% of the peak amplitude for that burst. Pharmacologically reactivated rhythms were described by averaging burst rates over a 2 min time period at steady state. Values are means ± SEM except for histological analyses (means ± SD). Significance ($p < 0.05$) was assessed by one-sample *t* test using Sigmaplot (Systat Software, Point Richmond, CA).

Results

Anatomical relationship between neonatal rat brainstem nuclei and PBC

Inspiratory active medullary slices are most commonly obtained from rats between P0 and P4. They are generated either in approximate reference to gross anatomical features, such as the position of hypoglossal nerve roots or obex, or in more precise reference to brainstem marker nuclei visualized in transilluminated, transverse brain sections produced during cutting. The latter approach is more precise, but assumes a constant anatomical relationship between the functionally defined PBC and the marker nuclei (Schwarzacher et al., 1995) (Figs. 1, 2). We tested this assumption by comparing the rostrocaudal extensions of marker nuclei in P0, P2, and P4 SD and W rats. Convenient ventral marker nuclei include the facial motonucleus, the lateral reticular nucleus, and, in particular, different subnuclei of the inferior olive (Li et al., 2001). Less valuable information is obtained from dorsal structures such as the hypoglossal motonucleus or obex as their association with ventral structures is sensitive to the cutting angle ("tilt") (Fig. 2*A*). Ambigual motoneurons do not aggregate to a detectable nucleus in transverse 50–100 μm sections.

The marker nuclei were first studied in thionin-stained transverse serial sections (50 μm) from 15 agar-embedded fixed brain-

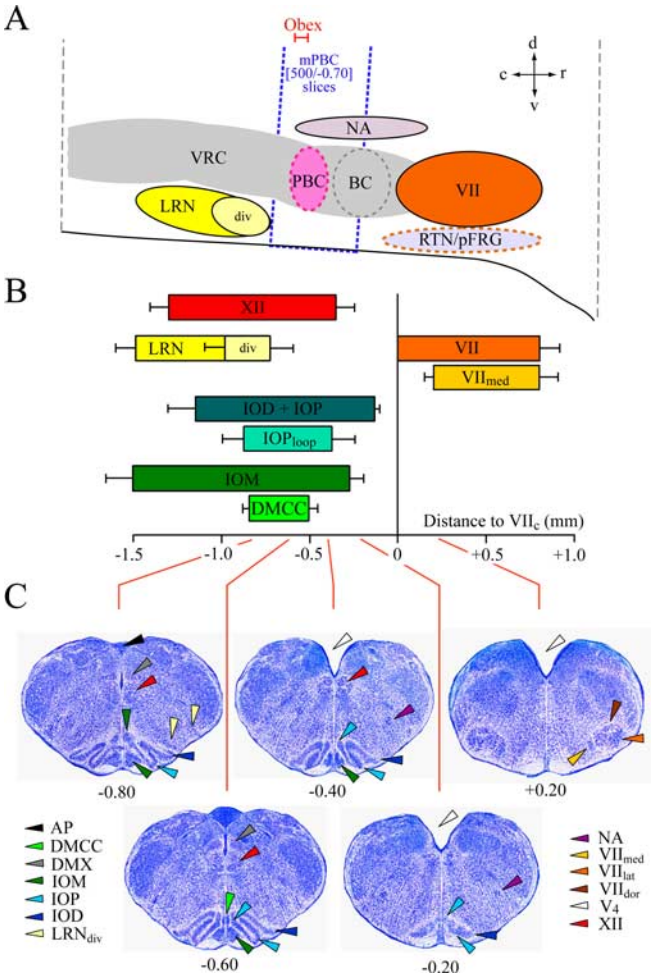

Figure 2. Ventral respiratory regions and respiratory marker nuclei. ***A***, Schematic sagittal section showing ventral respiratory regions [modified after Smith et al. (1991); Alheid et al. (2004)] and marker nuclei of Figure 1 *B*. The dotted box indicates the mean position of 500-μm-thick slices with the PBC in the middle ("mPBC") and mean boundaries at −0.70 and −0.20 mm, respectively (compare Figs. 3, 4). The position of obex (−0.55 VII_c) relative to PBC in transverse sections depends on sectioning angle (Fig. 3). The horizontal scale is the same as for ***B*** showing means (±SD) of rostrocaudal boundaries of marker nuclei from 15 fixed brainstems. ***C***, Sample transverse sections from W-P2 reference atlas (supplemental material, available at www.jneurosci.org) showing marker nuclei in ***A*** and ***B*** and additional structures. Abbreviations not used in Figure 1: VRC, ventral respiratory column; BC, Bötzinger complex; RTN, retrotrapezoid nucleus; pFRG, parafacial respiratory group; NA, nucleus ambiguus; VII_{dor}, dorsal subnucleus of VII; VII_{lat}, lateral subnucleus of VII; V_4, fourth ventricle.

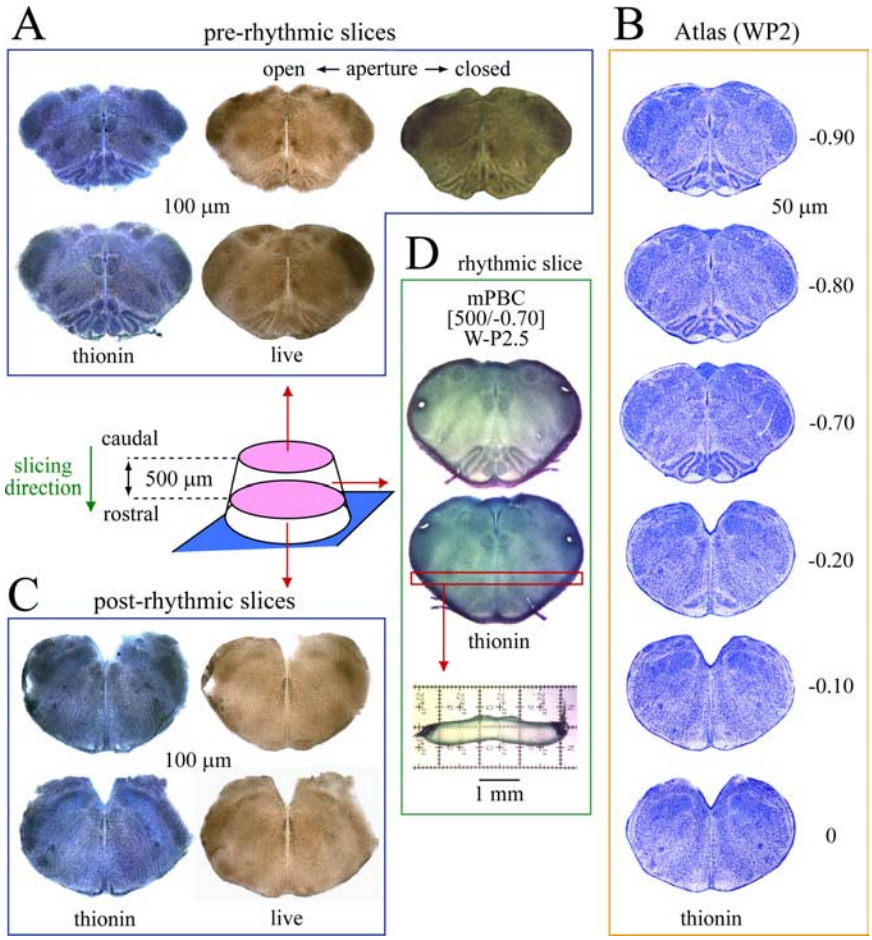

Figure 3. On-line histology for generating calibrated PBC slices. The diagram shows newborn rat brainstem glued with rostral side to metal plate attached to vibratome stage. Serial sectioning in caudorostral direction provides 100-μm-thin prerhythmic sections (***A***), which are compared with a W-P2 rat atlas (***B***) (supplemental material, available at www.jneurosci.org) to determine cutting level and caudal boundary of the rhythmic slice, in this case −0.70 mm relative to VII_c. As shown for the second-to-last prerhythmic slice (top row), resolution can be enhanced by adjusting the condensor aperture or focus. Sections are photographed, fixed for thionin staining, and rephotographed for higher resolution off-line analysis. ***C***, Postrhythmic slices taken after cutting the rhythmic slice are used for on- and off-line analysis of rostral slice boundary. ***D***, Fixed rhythmic slice stained with thionin to define caudal (top image) and rostral (bottom image) surfaces. The thickness of the rhythmic slice, here 500 μm, is determined by sectioning the horizontal strip at level of VRC/PBC. Combined on-line/off-line analysis revealed caudal and rostral slice boundaries at −0.70 and −0.20, respectively, and that the PBC is close to the middle of the slice (Fig. 2*A*). Sections in ***A***, ***C***, and ***D*** are from one individual WP2.5 brainstem. Thus, this calibrated PBC slice is described as "mPBC[500/−0.70]W-P2.5."

stems (Fig. 1). The position of each section was defined by its distance (in millimeters) from the caudal end of facial nucleus (VII_c) (Fig. 1*A*, left) (regions caudal to VII_c were assigned negative values). Living tissue from 11 brainstems was then sectioned serially (100 μm) in superfusate, photographed (Fig. 1*A*, middle), fixed, and stained with thionin, and then rephotographed (Figs. 1*A*, right). In these sets of serial sections, the rostrocaudal extensions of marker nuclei (Fig. 1*B*), as well as the distance from the rostral margin of the VII nucleus (VII_r) to the caudal margin of the medial inferior olivary nucleus (IOM_c) (Fig. 1*C*) was the same whether compared between rat strains (W vs SD), age groups (P0 vs P2 and P4), or live versus fixed sections. The anatomical relation of the marker nuclei with respiratory brainstem regions, specifically the parafacial respiratory group/retrotrapezoid nucleus complex and the VRC including the PBC and Bötzinger complex, are shown in Figure 2, *A* and *B*. The consistency of marker nuclei, both in absolute dimension and position relative to each other, allowed construction from one P2 W rat brainstem of a "reference atlas" comprising serial, transverse, 50 μm sections through the neonatal rat medulla that was applicable to SD and W rats between P0 and P4 (Fig. 2*C*; see also supplemental material, available at www.jneurosci.org).

On-line histology for generating calibrated PBC slices

Based on the constancy of brainstem anatomy for P0–P4 rats, we developed on-line histology, a method for generation and rapid documentation of PBC slices with defined boundaries. Brainstem sections were cut with a vibratome in the caudorostral direction starting at the caudal end of the inferior olive (Fig. 3). Section thickness was reduced to 100 μm when approaching the desired level for generating a rhythmic slice. Prerhythmic live sections were inspected on-line and photographed. Varying the focus or condensor aperture revealed medullary marker nuclei, especially subnuclei of the inferior olive (Fig. 3*A*). Sections were compared with the reference atlas (Fig. 3*B*) to evaluate, on-line, the rostrocaudal position. For defining the rostral border of the rhythmic slice, "postrhythmic" sections were cut and photographed (Fig. 3*C*). For more detailed "off-line" analysis of slice boundaries, prerhythmic and postrhythmic "frame" sections were fixed and stained with thionin (Fig. 3*A*,*C*).

Generation of calibrated 500-μm-thick PBC slices

We next tested whether on-line histology facilitates generation of rhythmic slices with predetermined and consistent rostrocaudal borders. We compared the actual versus desired rostrocaudal boundaries of 21 slices (500 μm thick) that were cut to have the caudal and rostral boundaries at −0.70 and −0.20 mm caudal to VII_c, respectively. This should place the center of the PBC (located at about −0.50 mm) (Smith et al., 1991) near the middle of such slices (Figs. 2–4), to be described as mPBC[500/−0.70]SD/W-P0/4 (mPBC, PBC in the middle; 500 indicates thickness in micrometers; −0.70 refers to caudal boundary relative to VII_c; SD/W-P0/4, 0- to 4-d-old SD or W rats). Slice thickness was determined by sectioning a horizontal strip at the level of the VRC/PBC (Fig. 3*D*). Values were similar in freshly cut (560 ± 12 μm; $n = 3$) and fixed slices (518 ± 38 μm; $n = 7$) (Fig. 4*A*), indicating minimal shrinkage during fixation. Sectioning for physical thickness also revealed that the dye penetrated <50 μm into the translucent brainstem tissue (Fig. 3*D*). Thus, identification of transection level based on analysis of stained surface structures in rhythmic and frame slices should be accurate within 50 μm. Caudal and rostral slice boundaries determined by analyzing surface structures in the rhythmic slices (Fig. 3*D*) averaged −0.70 ± 0.05 and −0.20 ± 0.09 ($n = 21$), respectively (Fig. 4*A*). Because these values were very close to the targeted values, we propose that rostrocaudal boundaries of PBC slices can be accu-

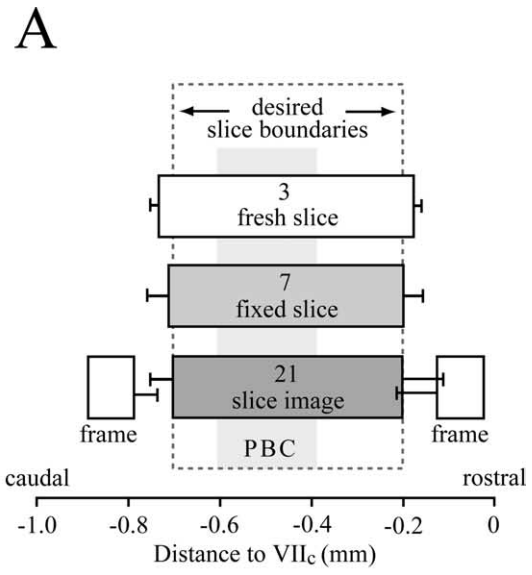

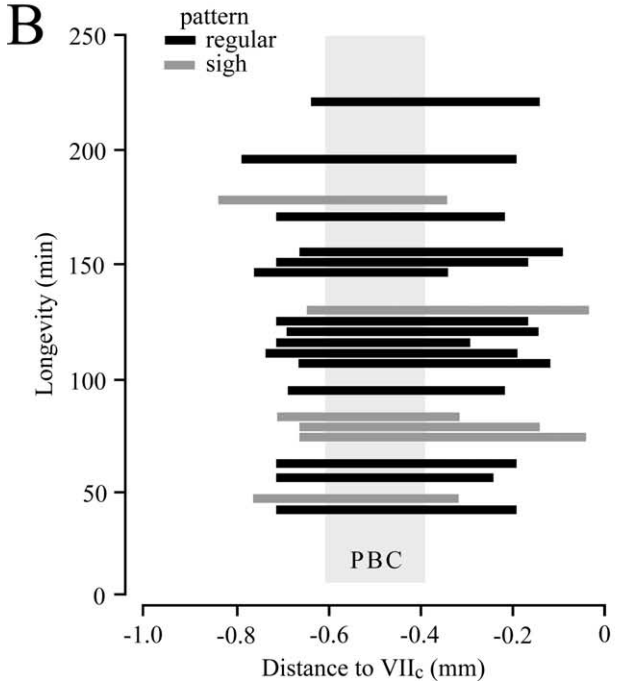

Figure 4. Boundaries and dimensions of mPBC[500/−0.70]SD/W-P0/4 slices versus longevity of rhythm in 3 mM [K^+] solution. ***A***, Means (±SD) of rostral and caudal slice boundaries (slice image) determined in 21 slices in relation to atlas (supplemental material, available at www.jneurosci.org). Caudal and rostral frame values were similarly obtained from last prerhythmic and first postrhythmic slices, respectively (for details, see Fig. 3). The location and physical thickness of seven fixed, thionin-stained slices ("fixed slice") are compared with three unfixed, unstained slices ("fresh slice") measured in standard superfusate within 20 min of preparation. Note gaps between slice boundaries determined from analysis of rhythmic slices compared with frame sections. ***B***, Plot of rostrocaudal boundaries of slices versus longevity of rhythm (Fig. 5). Most slices showed a regular inspiratory pattern (dark bars) (Figs. 5, 6), whereas some showed sigh-like activity (gray bars) (Fig. 7).

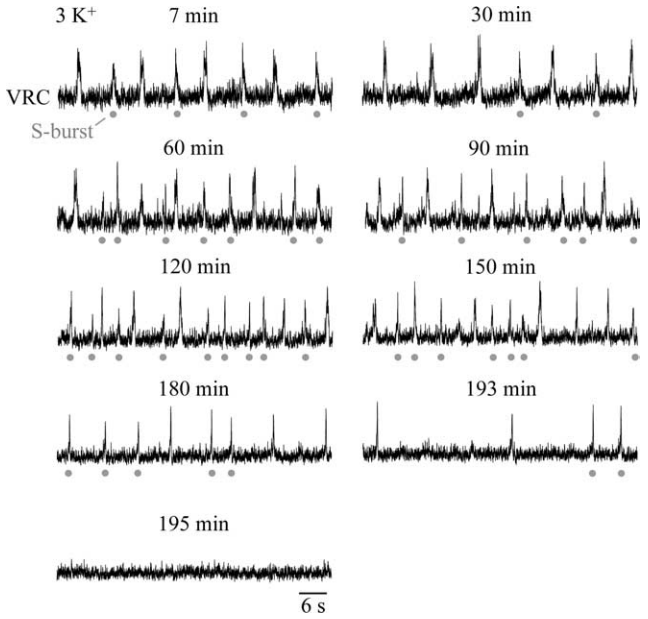

Figure 5. Inspiratory rhythm in 3 mM [K^+] superfusate. Suction electrode recording of VRC activity in a mPBC[500/−0.78]W-P0 slice producing regular rhythm. The frequency of VRC population activity varied between 8 and 13 bursts/min for a time period of 180 min, before rhythm slowed after 193 min and then stopped after 195 min. The gray circles indicate single bursts (S-bursts). Nonlabeled bursts are intermingled bursts (I-bursts) comprising two partially overlapping S-bursts.

rately quantified off-line by comparing their surface structures with those in the atlas.

Comparison of rhythmic slice boundaries with the position of the last prerhythmic and first postrhythmic slice revealed a rostrocaudal gap between surface structures in the rhythmic slice ("slice image") and the adjacent prerhythmic or postrhythmic frame sections of 89 ± 24 and 86 ± 58 μm ($n = 21$), respectively (Fig. 4*A*). This gap likely reflects tissue transparency, dye entry into rhythmic and frame slices, and possibly disintegration of a thin layer of tissue during slicing procedures. This gap has to be taken into account for generation of a rhythmic slice using online histology.

Rhythm in calibrated PBC slices at 3 mM [K^+]

Our next objective was to assess the activity of defined mPBC slices in solution of physiological [K^+]. Fifteen mPBC[500/−0.70]SD/W-P0/4 slices generated regular inspiratory VRC rhythm for 142 ± 13 min (range, 53–221 min) (Fig. 5). Despite our original premise that rhythmic activity in 3 mM K^+ might be limited in slices with the PBC close to the surface, there was no obvious correlation between slice boundaries and longevity of rhythm (Fig. 4*B*). In fact, slices with the PBC near their rostral or caudal surfaces were among those with the greatest longevity. Whether longevity is reduced in slices with the PBC at the slice surface, however, requires additional investigation.

We then characterized whether longevity of rhythm depends on slice thickness. For this, we generated slices extending an additional ~50 μm in rostral and caudal directions ($n = 11$). These mPBC[600/−0.76]SD/W-P0/4 slices showed rhythm for 240 ± 25 min ($n = 8$; range, 126–322 min) thus for a notably longer time period than the above 500 μm slices. In the 500- and 600-μm-thick slices, mean inspiratory frequencies were 8.8 ± 0.8 ($n = 15$) and 8.1 ± 0.5 ($n = 8$) bursts/min at 20 min of recording. Burst rate typically remained rather constant until 10–20 min before arrest of rhythm (Fig. 6*A*,*B*). In 80% of mPBC[500/−0.70] slices, 1–15 single bursts ("S-bursts") of relatively uniform duration (0.61 ± 0.03 s; $n = 4$) alternated with bursts of similar amplitude that were of longer duration (0.80 ± 0.05 s; $n = 4$) and appeared to comprise two partially overlapping single, "intermingled" bursts ("I-bursts") (Fig. 5). In ~60% of those 500 μm slices, the duration of the I- and S-bursts began to decline

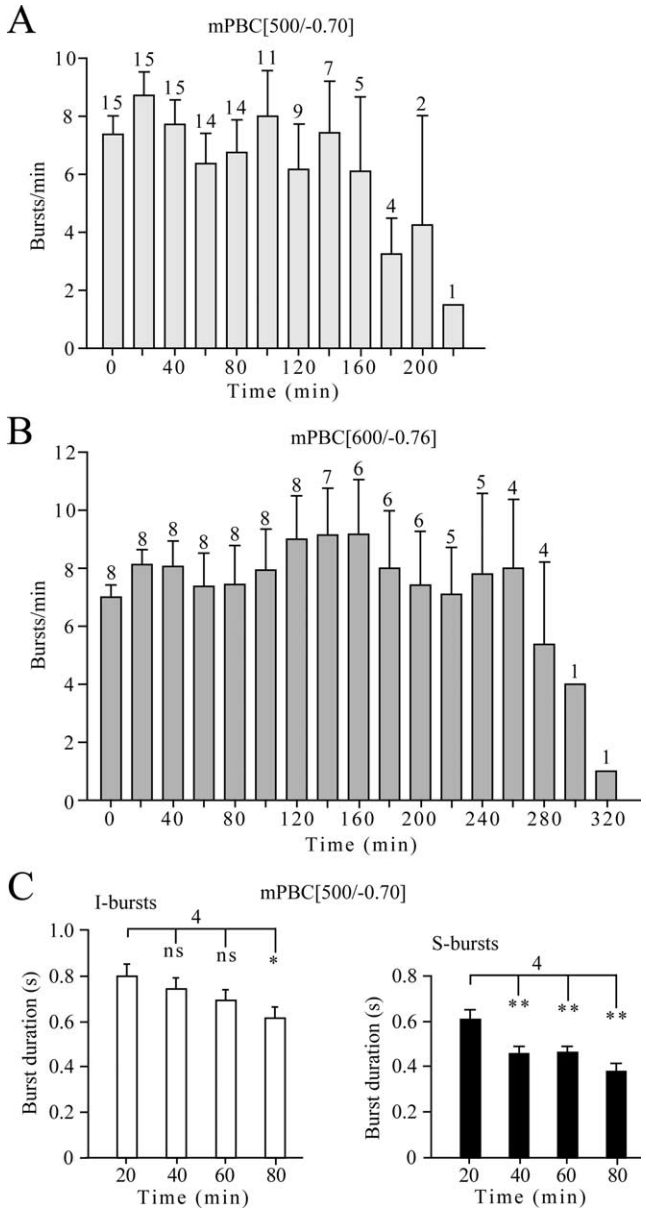

Figure 6. Time dependence of inspiratory burst frequency and duration. ***A***, ***B***, Burst rates in mPBC[500/−0.70] (***A***) and mPBC[600/−0.76] (***B***) slices. The digits indicate the number of slices [out of 15 (***A***) and 8 (***B***)] active at indicated time periods. ***C***, Duration of intermingled bursts (I-bursts, left) and single bursts (S-burst, right). Three consecutive bursts were analyzed for each time period in each slice. The bars represent means ± SEM; digits indicate the number of slices. $*p < 0.05$; $**p < 0.01$.

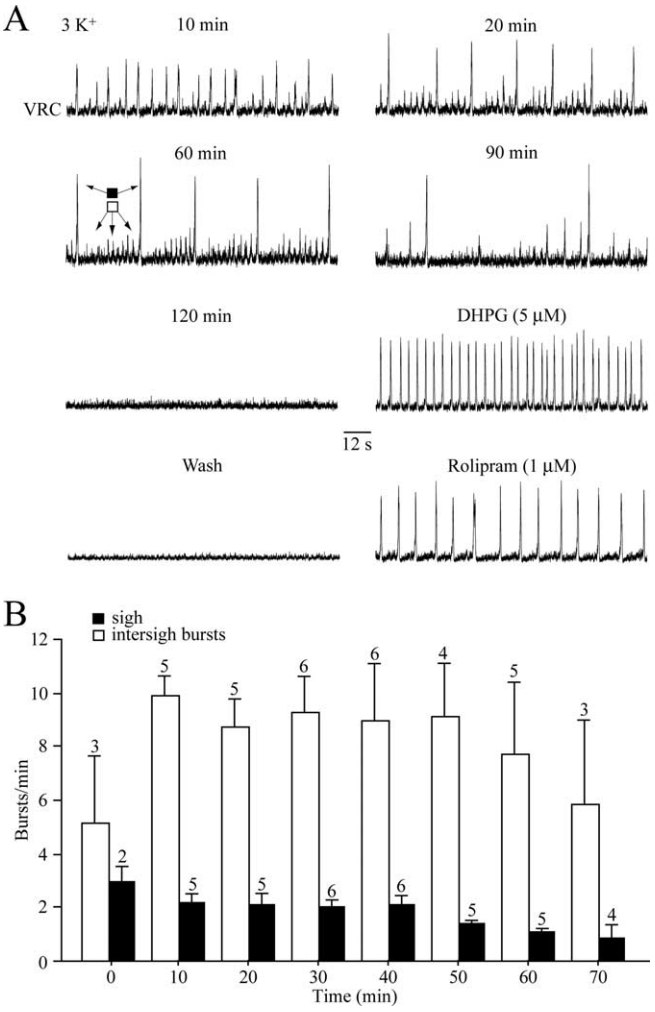

Figure 7. Sigh-like inspiratory activity. ***A***, In a mPBC[500/−0.73]W-P0 slice, an initially regular rhythm of small amplitude bursts transformed within 10 min into a pattern of single augmenting, sigh-like bursts followed by a period in which the burst amplitude cycled from a low-amplitude burst followed by four to eight bursts of progressively greater amplitude and one very large amplitude sigh-like burst that seemed to restart the cycle. After spontaneous arrest of rhythm after 120 min, regular inspiratory bursting was evoked by bath application of the group-I metabotropic glutamate receptor agonist DHPG and, after washout of DHPG, the inhibitor of cAMP-specific phosphodiesterase-4 rolipram. ***B***, Time dependence of mean sigh-like (black boxes) and intersigh (open boxes) burst frequencies in mPBC[500/−0.70] slices. The bars represent means ± SEM; values indicate the number of slices.

after >1 h and >20 min, respectively (Fig. 6*C*). The duration of both types of bursts typically remained stable for >2 h in mPBC[600/−0.76] slices.

Three of 11 mPBC[600/−0.76] and 6 of 21 mPBC[500/−0.70] slices developed "sigh-like" activity (Fig. 7*A*) (Lieske et al., 2000). Sigh-like bursts, which were larger in amplitude because of the occurrence of a second burst during the decaying phase of the initial burst, occurred at a rate of 2.1 ± 0.4 bursts/min ($n = 5$; at 20 min of recording) (Fig. 7*B*). They were often followed by a period of reduced activity during which burst amplitude decreased markedly (sometimes disappearing for brief periods) and then increased gradually during the next 3–12 consecutive intersigh bursts, which occurred with an average frequency of 8.7 ± 1.1 bursts/min at 20 min of recording ($n = 5$) (Fig. 7*B*). Longevity of sigh-like rhythm in 500 μm slices was 108 ± 12 min ($n = 6$).

Neuromodulation of PBC inspiratory networks

Inhibition by opiates

Bath application of DAMGO (10 nM), which decreases cellular cAMP via μ-opiate receptors (Ballanyi et al., 1997; Richter et al., 1997), lowered burst frequency to <20% of control (i.e., to 0–2 bursts/min in four mPBC[500/−0.70] slices), whereas 25 nM DAMGO abolished rhythm in mPBC[500/−0.70] ($n = 3$) and mPBC[600/−0.76] ($n = 3$) slices (Fig. 8). In the 600 μm slices, rhythm was effectively reactivated after combining washout of the drug with application of the μ-receptor antagonist naloxone (1 μM) (Fig. 8).

Neurostimulants

Our above data show that longevity of rhythm in 3 mM [K^+] superfusate increases with slice thickness consistent with the hypothesis that rundown of bursting reflects washout of endogenous excitatory neuromodulator(s). Given this observation, we assessed in the

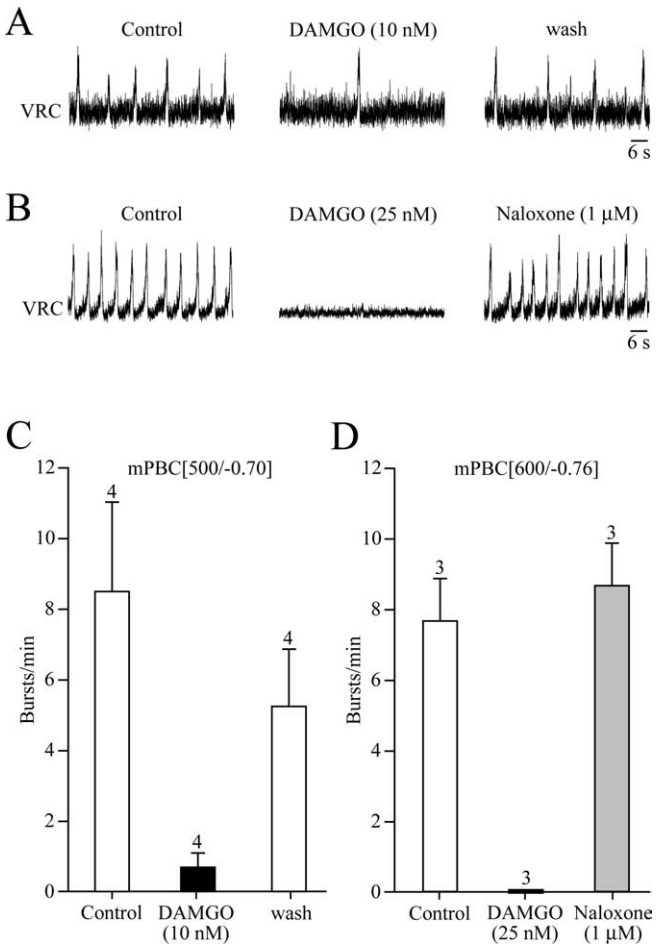

Figure 8. Opiate-induced depression of inspiratory rhythm. ***A***, In a mPBC[500/−0.77] W-P2 slice, bath application of the μ-opiate receptor agonist DAMGO depressed frequency, but not amplitude of inspiratory VRC bursting. Rhythm recovered partially after 25 min of washout. ***B***, In a mPBC[600/−0.80] W-P3 slice, DAMGO abolished rhythm, which was reactivated within 5 min of simultaneously washing out DAMGO while washing in (bath application) of the opiate receptor antagonist naloxone. ***C***, ***D***, Bar graphs show effects of DAMGO on frequency and the recovery of rhythm after washout of DAMGO alone (***C***) and in the presence of naloxone (***D***). The bars represent means ± SEM; values indicate the number of slices tested.

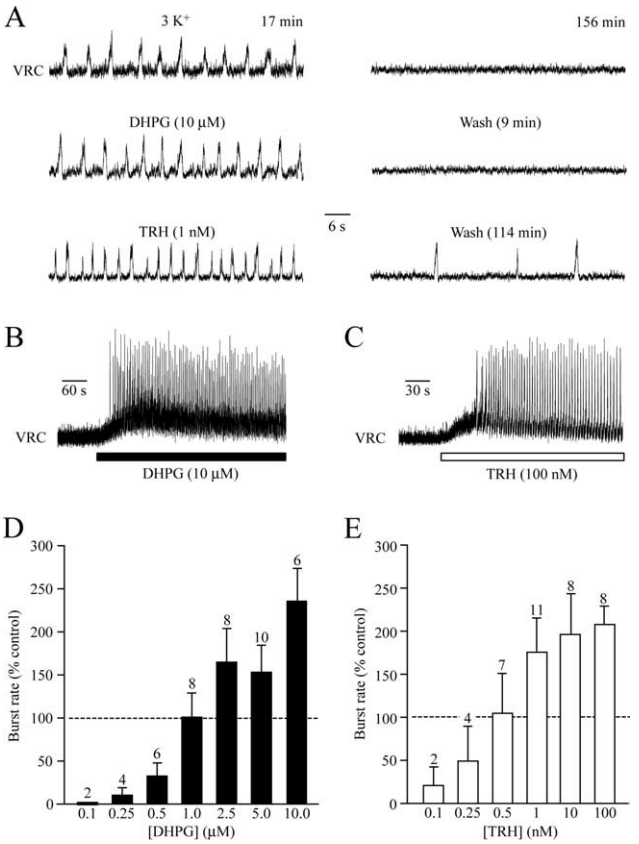

Figure 9. Neurotransmitter-evoked reversal of *in vitro* apnea. ***A***, Control activity in 3 mM [K^+] (left, top trace) spontaneously arrested after 156 min in a mPBC[500/−0.70]SD-P1.5 slice (right). Bath application of DHPG reactivated bursting activity very similar to control, which again stopped within 9 min of wash. A comparable rhythm was also elicited by TRH. Note that, in contrast to DHPG, bursting continued for almost 2 h after TRH washout. ***B***, ***C***, In the initial phases of bath application, DHPG (***B***) (10 μM; mPBC[500/−0.70]SD-P1.5) or TRH (***C***) (100 nM; mPBC[500/−0.70]W-P2) evoked tonic activity, as evidenced by a shift and increased thickness in the baseline of the integrated VRC signals. ***D***, ***E***, Bar graphs show that the efficacy of DHPG (***D***) and TRH (***E***) in reactivating inspiratory rhythm is strongly dose dependent. Note that 1 μM DHPG and 0.5 nM TRH evoke a rhythm similar to that observed in control solution. The bars represent means ± SEM; values indicate the number of preparations tested.

mPBC[500/−0.70] slices the ability to reactivate rhythm of neurostimulants acting on different signaling pathways.

Glutamate and metabotropic receptors

Bath application of 1 μM DHPG, a group-I metabotropic glutamate receptor agonist (Conn and Pin, 1997), reactivated rhythm with a pattern and frequency very similar to control (Fig. 9*A*,*B*,*D*). At threshold concentration (0.25 μM), rhythm returned at very low frequencies (<1 burst/min), whereas 10 μM DHPG evoked 17.1 ± 1.4 bursts/min ($n = 6$; maximum, 24) (Fig. 9*D*). In >50% of cases, 2.5–10 μM DHPG elicited tonic VRC activity initially (Fig. 9*B*). Rhythm persisted throughout drug administration periods of 15–20 min and typically disappeared within <15 min of starting washout of DHPG (Fig. 9*A*).

Thyrotropin-releasing hormone

Very similar results were obtained with TRH (Fig. 9*A*,*C*,*E*), which blocks K^+ channels via $G_{\alpha q}$ proteins (Chen et al., 2006). At 0.5 nM, TRH reactivated rhythm almost indiscernible from control. At threshold concentration (0.1 nM), TRH evoked <1 bursts/min, whereas frequency reached 17.2 ± 1.1 bursts/min ($n = 8$; maximum, 21) at 100 nM TRH (Fig. 9*E*). In three slices, 10–100 nM TRH induced tonic activity initially (Fig. 9*C*) and also decreased burst strength to 20–70% of the value of uniform bursting at lower concentrations in two cases. At all concentrations, the frequency of TRH-induced rhythm remained stable throughout the application period (15–20 min). In two slices, rhythm persisted for >1 h after start of washout (Fig. 9*A*).

Elevation of cAMP levels

We tested next effects of receptor-independent elevation of cellular cAMP induced by the phosphodiesterase-4 blocker rolipram and the less specific blocker theophylline (O'Donnell and Zhang, 2004). Inspiratory rhythm was reactivated to frequencies of 1.6 ± 0.7 ($n = 5$) and 5.4 ± 0.8 ($n = 8$) bursts/min by 0.25 and 2.5 mM theophylline, respectively (Fig. 10*A*,*C*). Rolipram, at 1 and 5 μM, also reactivated the arrested PBC network in the 500 μm slices, causing burst rate to increase to 6.1 ± 0.9 ($n = 11$) and 6.8 ± 2.3 bursts/min ($n = 3$), respectively (Fig. 10*B*,*C*). In six mPBC[600/−0.76] slices, 0.25 and 5 μM rolipram were comparably effective (6.3 ± 0.3 vs 6.9 ± 0.6 bursts/min) (Fig. 10*D*). At 1–5 μM, the action of rolipram persisted between 30 and 120 min after washout of the agent (Fig. 10*B*). Theophylline and rolipram

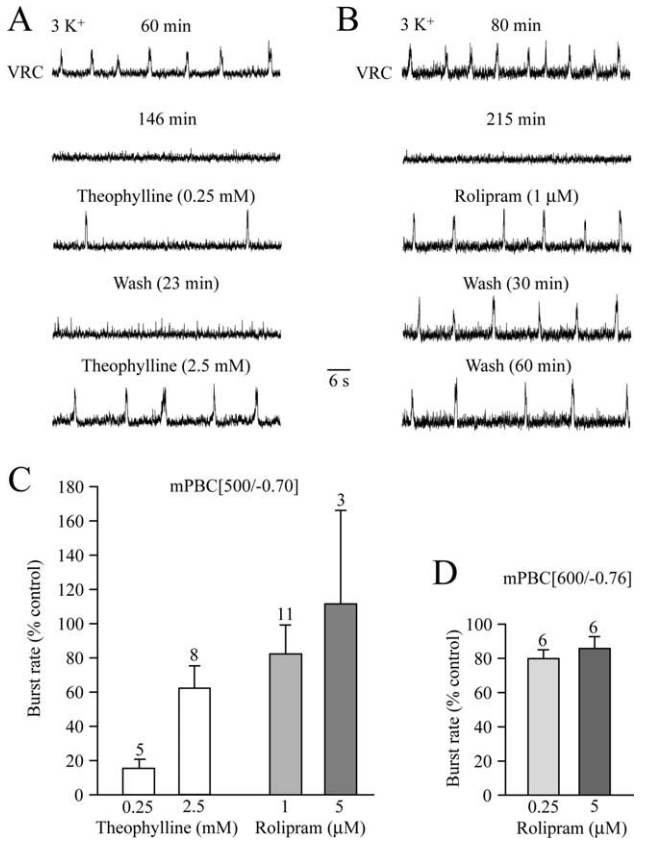

Figure 10. Reversal of *in vitro* apnea by cAMP-elevating phosphodiesterase-4 blockers. ***A***, After spontaneous arrest of inspiratory bursting in a mPBC[500/−0.68]SD-P0.5 slice after 146 min, a low-frequency rhythm was evoked by the nonspecific blocker of cAMP-specific phosphodiesterase-4, theophylline. A 10-fold increase in theophylline concentration to 2.5 mM raised frequency ~2.5-fold. ***B***, The specific phosphodiesterase-4 blocker rolipram reactivated rhythm in a mPBC[500/−0.63]W-P2 slice. The stimulating action of rolipram persisted for >1 h after washout. ***C***, Histograms summarizing the dose-dependent stimulatory effects of theophylline and rolipram on quiescent mPBC[500/−0.70] slices. ***D***, Histogram summarizing effects of rolipram on quiescent mPBC[600/−0.76] slices. Note that nanomolar concentrations of rolipram reactivate rhythm at rates similar to controls. The bars represent means ± SEM; values indicate the number of slices.

did not typically induce tonic activity. Although lower in frequency, these drugs often elicited more robust and regular bursting than DHPG and TRH.

All neurostimulators also evoked regular rhythm in four slices with sigh pattern (Fig. 7).

Ca^{2+} imaging of neuromodulator-induced rhythmic activities in assemblies of VRC/PBC neurons

Our electrophysiological VRC approach was not suited to study whether rhythmic behaviors elicited by the above agents stimulate the same VRC/PBC neurons. Consequently, we combined electrophysiological recording with Ca^{2+} imaging for assessment within the contralateral VRC/PBC of activity and morphology of groups of individual neurons. In eight mPBC[500/−0.69] slices, recordings were done from 17 PBC cells located between −0.60 and −0.58, thus within the caudal PBC boundary and 34 non-PBC VRC cells located between −0.78 and −0.69 (compare Fig. 2*A*). Somata of these cells showed Ca^{2+} rises in phase with VRC/PBC rhythm (Figs. 11, 12; see also movie in supplemental material, available at www.jneurosci.org). In <15% of cells, Ca^{2+} oscillations were also apparent in proximal dendrites. Neurons with higher resting fluorescence intensity typically showed larger inspiratory-related Ca^{2+} oscillations. The vast majority of neurons initially active in 3 mM $[K^+]$ showed very similar Ca^{2+} rises when rhythm was reactivated with DHPG (87.8%; $n = 41$), TRH (70.6%; $n = 34$), rolipram (84.2%; $n = 19$), or theophylline (94.1%; $n = 17$) (Figs. 11, 12). *z*-stack image series enabled 3D-animated movies (supplemental material, available at www.jneurosci.org), which revealed basic morphological features of VRC (Fig. 11) and PBC neurons (Fig. 12) such as soma shape and number of primary dendrites.

Discussion

We have analyzed for the first time endogenous rhythm at physiological extracellular $[K^+]$ in brainstem slices containing the PBC inspiratory center. These slices with well defined rostrocaudal boundaries were highly sensitive to neuromodulators. Activity of localized and functionally identified PBC neurons and reactivation of their rhythmic discharge via distinct second-messenger pathways after spontaneous *in vitro* apnea was assessed with two-photon/confocal Ca^{2+} imaging.

Calibrated PBC slices

We found that the rostrocaudal extensions of respiratory marker nuclei (i.e., facial nucleus, lateral reticular nucleus, inferior olive) are remarkably constant in newborn rats. This enabled use of a reference rat brainstem atlas for generation of PBC slices with predictable and reproducible boundaries. Our on-line histological approach is a valuable step toward standardizing slicing procedures and provides a reference for comparison of results between laboratories. It will also form a reference for exploring the modification of PBC function by surrounding brainstem structures such as the parafacial respiratory group and the retrotrapezoid nucleus, which both overlap with the facial motonucleus (Fig. 2*A*) and contain chemosensitive neurons that presumably drive the PBC (Onimaru and Homma, 2003; Mulkey et al., 2004; Kawai et al., 2006). Here, we showed that the PBC is capable to generate rhythm at physiological $[K^+]$ without drive from these areas not included in mPBC[500/−0.70] slices.

High sensitivity to neuromodulators of rhythm in 3 mM $[K^+]$

The original report on the PBC stated briefly that >500-μm-thick slices can be active at physiological extracellular $[K^+]$ (Smith et al., 1991; Funk et al., 1993). Here, 600- and 500-μm-thick slices with the PBC in the center generated inspiratory rhythm for ~4 and >2 h, respectively, at frequencies comparable with those of slices in elevated $[K^+]$. Similar to the *in situ* perfused brainstem preparation (Manzke et al., 2003), the rhythm was blocked by low nanomolar concentrations of μ-agonist, whereas micromolar concentrations are typically necessary to abolish slice rhythms in high $[K^+]$ superfusate (Johnson et al., 1994). This indicates that K^+ counteracts depressant effects of inhibitory neuromodulators in PBC slices by unspecifically increasing neuronal excitability (Somjen, 2002).

The PBC network in the calibrated slices is also very sensitive to excitatory neuromodulators. TRH is often used at high nanomolar to micromolar concentrations to reveal stimulatory effects on (respiratory) brainstem slices (Funk et al., 1994; Rekling et al., 1996; Browning and Travagli, 2001). Here, picomolar TRH concentrations could already reactivate regular rhythm after spontaneous arrest, whereas 0.5 nM TRH mimicked rhythm in PBC slices before arrest. Regarding the mechanism of action, TRH targets $G_{\alpha q}$-protein-linked receptors that may directly block two-pore-domain K^+ channels (Chen et al., 2006; Töpert et al., 1998) that are proposed to contribute to respiratory rhythm generation (Ballanyi et al., 1999; Smith et al., 2000). While the respiratory stimulatory action of TRH is established (Hedner et al., 1983;

Bennet et al., 1988), we report for the first time that DHPG-mediated activation of metabotropic glutamate receptors induces PBC rhythm. Locomotor networks in neonatal rats (Nistri et al., 2006) and respiratory networks in lampreys (Bongianni et al., 2002) are similarly sensitive to the agent. Furthermore, DHPG augments L-type Ca^{2+} channel currents in unidentified VRC/PBC neurons (Mironov and Richter, 1998) and enhances the excitability of respiratory motoneurons (Dong and Feldman, 1999; Nistri et al., 2006). Our data suggest that glutamate may act endogenously through group-I metabotropic receptors coupled to phospholipase-C inositol-1,4,5-triphosphate signaling (Conn and Pin, 1997) to stimulate breathing.

The increased longevity of rhythm in thicker slices is consistent with the hypothesis that *in vitro* apnea reflects washout of excitatory agents. However, our findings do not allow the conclusion that the rhythm arrests because of washout of glutamate and/or TRH from the slices. Also, depletion of substance P from presynaptic terminals abolishes the slice rhythm (Morgado-Valle and Feldman, 2004), whereas substance P reactivates bursting after its arrest after lowering superfusate $[K^+]$ from 8 to 3 mM (Pena and Ramirez, 2004). Neuromodulator(s) acting through the cAMP–protein kinase A pathway, such as norepinephrine or serotonin (Richter et al., 1997; Manzke et al., 2003), may also be among the excitatory agent(s) that appear to be washed out from the slices. This is indicated by the stimulatory effects on the slice rhythm of theophylline and rolipram, which both inhibit cAMP-specific phosphodiesterase-4, resulting in a rise of cellular cAMP (Nikulina et al., 2004; O'Donnell and Zhang, 2004). While theophylline is commonly used clinically to reverse apneas in (preterm) infants, the antidepressant rolipram (O'Donnell and Zhang, 2004) antagonizes *in vitro* respiratory depression in perinatal rats (Ballanyi, 2004; Ruangkittisakul and Ballanyi, 2006). Here, theophylline stimulated the PBC network at low millimolar concentrations, whereas 250 nM rolipram already reactivated rhythm with rates only slightly lower than in controls. This rolipram concentration may be similar to or lower than those exerting beneficial effects on age-related memory deficits (Barad, 2003) and depression (O'Donnell and Zhang, 2004). Because rolipram-evoked rhythm was regular and robust, this or more recent phosphodiesterase-4 inhibitors with fewer side effects (Dal Piaz and Giovannoni, 2000; O'Donnell and Zhang, 2004) may effectively stimulate breathing in intact animals or humans.

The observation that all agents were comparably effective suggests that rhythmogenic PBC neurons and/or neurons providing tonic excitatory drive to these cells (Richter et al., 1992; Feldman et al., 2003) are targeted by multiple signaling pathways (Richter et al., 1997). This shows that washout of rhythm from PBC slices in 3 mM $[K^+]$ is not necessarily an obstacle to study the neural control of breathing. Rather, it enables both the identification of second-messenger pathways that can promote rhythm generation and the analysis of how these signaling cascades interact to modulate the rhythm. In that regard, the sigh-like inspiratory pattern (Lieske et al., 2000) *in vitro* may be associated with the hormonal status of pups resulting in an imbalance of endogenous neuromodulators. Interstitial levels of TRH, which facilitates regular rhythm in PBC slices, may be lower in poorly lactated animals (Nillni et al., 2001), resulting in a relative dominance of endogenous neuromodulator(s) promoting sighs, probably involving substance P (Shvarev et al., 2003).

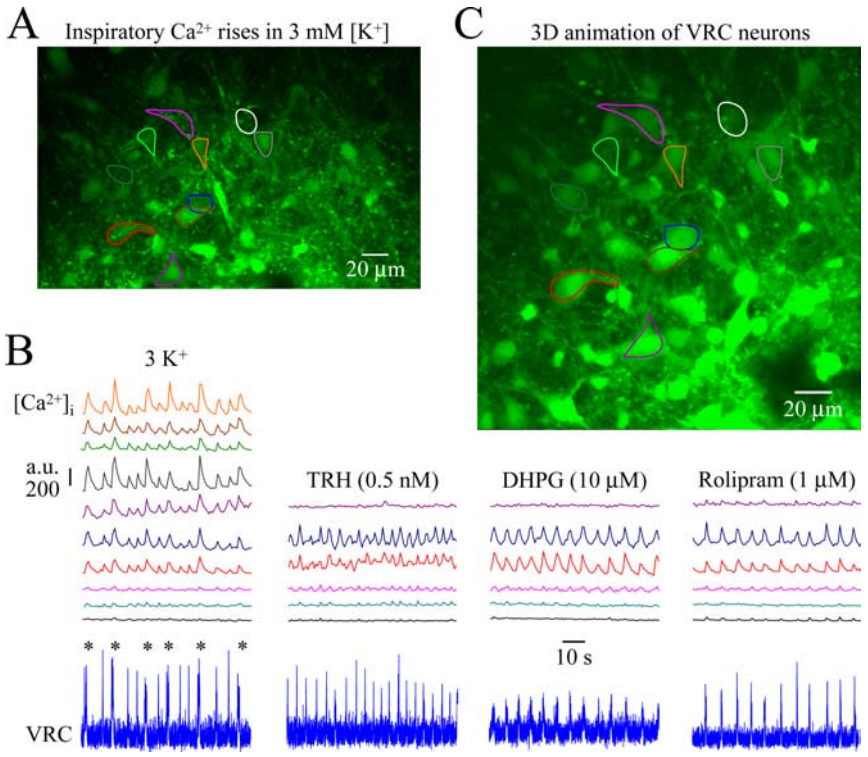

Figure 11. Confocal imaging of activity and morphology of inspiratory VRC neurons. ***A***, Cells in the VRC region of mPBC[500/−0.75] W-P3 slice stained after pressure injection with the Ca^{2+}-sensitive dye fluo-4-AM. Cells showing inspiratory-related increases of fluo-4 fluorescence, outlined as regions of interest, were located at a depth of 30 μm (i.e., −0.72 mm caudal to VII_c). ***B***, Eighty second simultaneous recordings in 3 mM $[K^+]$ of rhythmic Ca^{2+} oscillations plotted as fluorescence intensity in arbitrary units (a.u.) in identified VRC neurons in ***A*** and electrophysiological population activity in the contralateral VRC (bottom trace). Note that fluorescence increases were consistently larger during intermingled (I-bursts; asterisk) compared with single (S)-bursts (see supplemental movie, available at www.jneurosci.org as supplemental material; compare Figs. 5, 6). After washout of rhythm in 3 mM $[K^+]$, VRC bursting and Ca^{2+} oscillations were consecutively reactivated by TRH, DHPG, or rolipram. Note that cells represented by the top four traces in the left panel were not monitored during drug application because of a minor shift in focal plane over time. ***C***, 3D animation (supplemental material, available at www.jneurosci.org) showing gross morphology of VRC inspiratory neurons and nonrhythmic cells obtained from *z*-stack (0.5 μm single step) image series encompassing areas starting 7.5 μm above to 7.5 μm below the image plane of ***A***.

Imaging of VRC/PBC neurons

Similar to a current lack of knowledge on anatomical slice boundaries, the rostrocaudal location of electrophysiologically recorded respiratory neurons has not been reconstructed in by far most studies on rodent PBC slices. Accordingly, a significant portion of cells referred to as PBC neurons possibly comes from regions outside the PBC. In our study, all active cells at identified rostrocaudal levels showed Ca^{2+} rises during inspiratory VRC bursting with no indication of activity associated with other respiratory phases. Because no ratiometric Ca^{2+} dye was used here, no attempt was made to quantify the Ca^{2+} rises. Because glutamate evoked notably larger Ca^{2+} signals, the inspiratory Ca^{2+} transients may be rather modest (100–200 nM) as estimated by fura-2

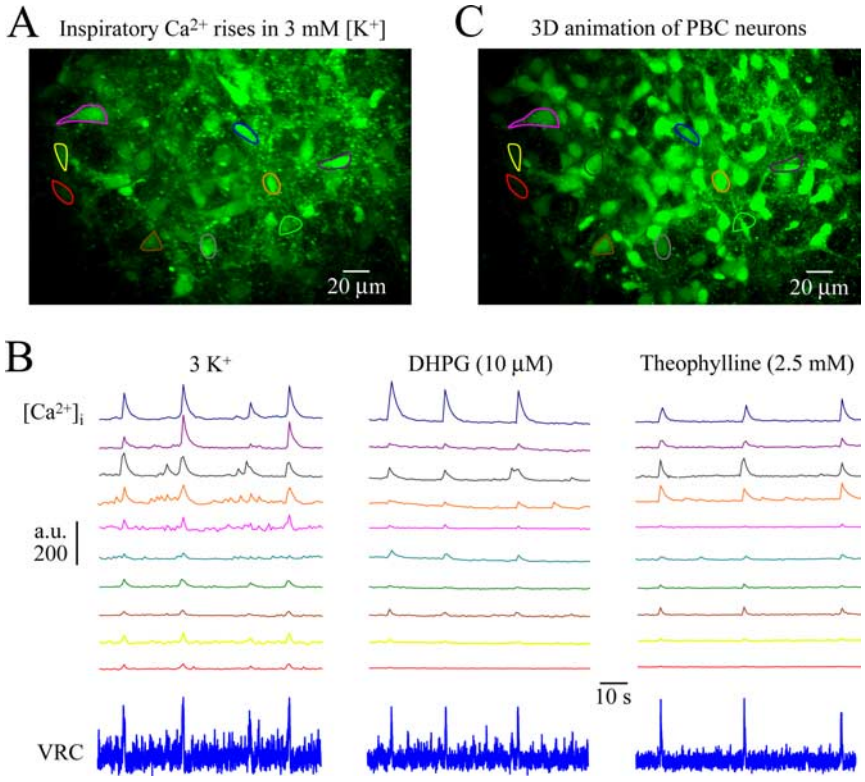

Figure 12. Confocal imaging of activity and morphology of inspiratory PBC neurons. ***A***, Fluo-4-AM-stained PBC neurons outlined by regions of interest at −0.59 in a mPBC[500/−0.64] W-P1.5 slice. The supplemental movie (available at www.jneurosci.org as supplemental material) shows 90 s recording in 3 mM [K^+] of rhythmic Ca^{2+} oscillations in these neurons that are in phase with inspiratory population activity recorded from the contralateral PBC (***B***, bottom left trace). ***B***, Fluo-4-AM fluorescence intensity is plotted in arbitrary units (a.u.) against time. After washout of rhythm in 3 mM [K^+], PBC bursting and Ca^{2+} oscillations were reactivated by DHPG and theophylline. ***C***, 3D animation (supplemental material, available at www.jneurosci.org) showing gross morphology of PBC neurons and neighboring nonrhythmic cells obtained from *z*-stack image series (0.5 μm single step) encompassing areas starting 7.5 μm above to 7.5 μm below image plane of ***A***.

Ca^{2+} measurements in unidentified VRC/PBC neurons (Frermann et al., 1999). Dialysis via the patch electrode with Ca^{2+} dye as in the latter study is one potent approach to reveal structural features of respiratory neurons. A unique advantage of our approach is that populations of neurons can be imaged after pressure injection of dye (Stosiek et al., 2003) into the VRC/PBC. A similar approach has been used previously (Koshiya and Smith, 1999), whereas another study loaded PBC slices from mice after bath application of membrane-permeable Ca^{2+} dye (Thoby-Brisson et al., 2005). Confocal imaging in our study afforded high spatial resolution and 3D images of neuronal networks within the VRC/PBC (Figs. 11, 12) as prerequisites for a structure–function relationship of the PBC.

A most important finding is that the same population of neurons that showed rhythmic Ca^{2+} rises in 3 mM [K^+] solution was reactivated by the neurostimulants. This suggests either that the agents (1) reactivate rhythm through a common population of rhythmogenic PBC neurons, (2) activate distinct pools of neurons that drive a common set of rhythmogenic PBC neurons that we imaged, or (3) activate distinct pools of rhythmogenic PBC neurons that converge on a common set of follower neurons that we imaged. We were unable to distinguish between these possibilities because optical recording in this study was restricted to tissue depths <70 μm for confocal imaging and <100 μm for two-photon imaging. The critical rostrocaudal boundaries of the newborn rat PBC have not yet been determined in slices but its center is hypothesized (Smith et al., 1991) to be close to −0.50 following the terminology introduced here (Fig. 2, 3) and extend ~100 μm in rostral and caudal directions. Accordingly, only a subpopulation of cells studied here represents "real" PBC neurons, which did not show major differences in gross morphology (i.e., soma shape and size or array of primary dendrites among each other or compared with VRC cells). Recording from cells in slices with the PBC more exposed to the caudal or rostral surface may reveal a morphology specific to rhythmogenic neurons. Additional criteria such as (fluorescent) tagging for PBC neuronal markers such as characteristic neurotransmitter receptors and transporters (Gray et al., 1999; Guyenet et al., 2004; Pagliardini et al., 2005) may facilitate the identification and analysis of the cellular rhythm generator.

References

Alheid GF, Milsom WK, McCrimmon DR (2004) Pontine influences on breathing: an overview. Respir Physiol Neurobiol 143:105–114.

Ballanyi K (2004) Neuromodulation of the perinatal respiratory network. Curr Neuropharmacol 2:221–243.

Ballanyi K, Lalley PM, Hoch B, Richter DW (1997) cAMP-dependent reversal of opioid- and prostaglandin-mediated depression of the isolated respiratory network in newborn rats. J Physiol (Lond) 504:127–134.

Ballanyi K, Onimaru H, Homma I (1999) Respiratory network function in the isolated brainstem-spinal cord of newborn rats. Prog Neurobiol 59:583–634.

Barad M (2003) Later developments: molecular keys to age-related memory impairment. Alzheimer Dis Assoc Disord 17:168–176.

Bennet L, Gluckman PD, Johnston BM (1988) The central effects of thyrotropin-releasing hormone on the breathing movements and electrocortical activity of the fetal sheep. Pediatr Res 23:72–75.

Bongianni F, Mutolo D, Carfi M, Pantaleo T (2002) Group I and II metabotropic glutamate receptors modulate respiratory activity in the lamprey. Eur J Neurosci 16:454–460.

Browning KN, Travagli RA (2001) The peptide TRH uncovers the presence of presynaptic 5-HT1A receptors via activation of a second messenger pathway in the rat dorsal vagal complex. J Physiol (Lond) 531:425–435.

Chen X, Talley EM, Patel N, Gomis A, McIntire WE, Dong B, Viana F, Garrison JC, Bayliss DA (2006) Inhibition of a background potassium channel by G_q protein alpha-subunits. Proc Natl Acad Sci USA 103:3422–3427.

Conn PJ, Pin JP (1997) Pharmacology and functions of metabotropic glutamate receptors. Annu Rev Pharmacol Toxicol 37:205–237.

Dal Piaz V, Giovannoni MP (2000) Phosphodiesterase 4 inhibitors, structurally unrelated to rolipram, as promising agents for the treatment of asthma and other pathologies. Eur J Med Chem 35:463–480.

Dong XW, Feldman JL (1999) Distinct subtypes of metabotropic glutamate receptors mediate differential actions on excitability of spinal respiratory motoneurons. J Neurosci 19:5173–5184.

Feldman JL, Del Negro CA (2006) Looking for inspiration: new perspectives on respiratory rhythm. Nat Rev Neurosci 7:232–242.

Feldman JL, Mitchell GS, Nattie EE (2003) Breathing: rhythmicity, plasticity, chemosensitivity. Annu Rev Neurosci 26:239–266.

Frermann D, Keller BU, Richter DW (1999) Calcium oscillations in rhythmically active respiratory neurones in the brainstem of the mouse. J Physiol (Lond) 515:119–131.

Funk GD, Smith JC, Feldman JL (1993) Generation and transmission of

respiratory oscillations in medullary slices: role of excitatory amino acids. J Neurophysiol 70:1497–1515.
Funk GD, Smith JC, Feldman JL (1994) Development of thyrotropin-releasing hormone and norepinephrine potentiation of inspiratory-related hypoglossal motoneuron discharge in neonatal and juvenile mice in vitro. J Neurophysiol 72:2538–2541.
Gray PA, Rekling JC, Bocchiaro CM, Feldman JL (1999) Modulation of respiratory frequency by peptidergic input to rhythmogenic neurons in the preBotzinger complex. Science 286:1566–1568.
Gray PA, Janczewski WA, Mellen N, McCrimmon DR, Feldman JL (2001) Normal breathing requires preBotzinger complex neurokinin-1 receptor-expressing neurons. Nat Neurosci 4:927–930.
Guyenet PG, Stornetta RL, Weston MC, McQuiston T, Simmons JR (2004) Detection of amino acid and peptide transmitters in physiologically identified brainstem cardiorespiratory neurons. Auton Neurosci 114:1–10.
Hedner J, Hedner T, Wessberg P, Lundberg D, Jonason J (1983) Effects of TRH and TRH analogues on the central regulation of breathing in the rat. Acta Physiol Scand 117:427–437.
Johnson SM, Smith JC, Funk GD, Feldman JL (1994) Pacemaker behavior of respiratory neurons in medullary slices from neonatal rat. J Neurophysiol 72:2598–2608.
Kawai A, Onimaru H, Homma I (2006) Mechanisms of CO_2/H^+ chemoreception by respiratory rhythm generator neurons in the medulla from newborn rats in vitro. J Physiol (Lond) 572:525–537.
Koshiya N, Smith JC (1999) Neuronal pacemaker for breathing visualized in vitro. Nature 400:360–363.
Li YX, Tokuyama W, Okuno H, Miyashita Y, Hashimoto T (2001) Differential induction of brain-derived neurotrophic factor mRNA in rat inferior olive subregions following unilateral labyrinthectomy. Neuroscience 106:385–394.
Lieske SP, Thoby-Brisson M, Telgkamp P, Ramirez JM (2000) Reconfiguration of the neural network controlling multiple breathing patterns: eupnea, sighs and gasps. Nat Neurosci 3:600–607.
Manzke T, Guenther U, Ponimaskin EG, Haller M, Dutschmann M, Schwarzacher S, Richter DW (2003) 5-$HT_{4(a)}$ receptors avert opioid-induced breathing depression without loss of analgesia. Science 301:226–229.
Mironov SL, Richter DW (1998) L-type Ca^{2+} channels in inspiratory neurones of mice and their modulation by hypoxia. J Physiol (Lond) 512:75–87.
Morgado-Valle C, Feldman JL (2004) Depletion of substance P and glutamate by capsaicin blocks respiratory rhythm in neonatal rat in vitro. J Physiol (Lond) 555:783–792.
Mulkey DK, Stornetta RL, Weston MC, Simmons JR, Parker A, Bayliss DA, Guyenet PG (2004) Respiratory control by ventral surface chemoreceptor neurons in rats. Nat Neurosci 7:1360–1369.
Nikolenko V, Nemet B, Yuste R (2003) A two-photon and second-harmonic microscope. Methods 30:3–15.
Nikulina E, Tidwell JL, Dai HN, Bregman BS, Filbin MT (2004) The phosphodiesterase inhibitor rolipram delivered after a spinal cord lesion promotes axonal regeneration and functional recovery. Proc Natl Acad Sci USA 101:8786–8790.
Nillni EA, Aird F, Seidah NG, Todd RB, Koenig JI (2001) PreproTRH(178–199) and two novel peptides (pFQ7 and pSE14) derived from its processing, which are produced in the paraventricular nucleus of the rat hypothalamus, are regulated during suckling. Endocrinology 142:896–906.
Nistri A, Ostroumov K, Sharifullina E, Taccola G (2006) Tuning and playing a motor rhythm: how metabotropic glutamate receptors orchestrate generation of motor patterns in the mammalian central nervous system. J Physiol (Lond) 572:323–334.
O'Donnell JM, Zhang HT (2004) Antidepressant effects of inhibitors of cAMP phosphodiesterase (PDE4). Trends Pharmacol Sci 25:158–163.
Onimaru H, Homma I (2003) A novel functional neuron group for respiratory rhythm generation in the ventral medulla. J Neurosci 23:1478–1486.
Onimaru H, Ballanyi K, Richter DW (1996) Calcium-dependent responses in neurons of the isolated respiratory network of newborn rats. J Physiol (Lond) 491:677–695.
Onimaru H, Ballanyi K, Homma I (2003) Contribution of Ca^{2+}-dependent conductances to membrane potential fluctuations of medullary respiratory neurons of newborn rats in vitro. J Physiol (Lond) 552:727–741.
Pagliardini S, Adachi T, Ren J, Funk GD, Greer JJ (2005) Fluorescent tagging of rhythmically active respiratory neurons within the pre-Botzinger complex of rat medullary slice preparations. J Neurosci 25:2591–2596.
Pena F, Ramirez JM (2004) Substance P-mediated modulation of pacemaker properties in the mammalian respiratory network. J Neurosci 24:7549–7556.
Rekling JC, Champagnat J, Denavit-Saubie M (1996) Thyrotropin-releasing hormone (TRH) depolarizes a subset of inspiratory neurons in the newborn mouse brain stem in vitro. J Neurophysiol 75:811–819.
Richter DW, Spyer KM (2001) Studying rhythmogenesis of breathing: comparison of in vivo and in vitro models. Trends Neurosci 24:464–472.
Richter DW, Ballanyi K, Schwarzacher S (1992) Mechanisms of respiratory rhythm generation. Curr Opin Neurobiol 2:788–793.
Richter DW, Lalley PM, Pierrefiche O, Haji A, Bischoff AM, Wilken B, Hanefeld V (1997) Intracellular signal pathways controlling respiratory neurons. Respir Physiol 110:113–123.
Ruangkittisakul A, Ballanyi K (2006) Reversal by phosphodiesterase-4 blockers of in vitro apnea in the isolated brainstem-spinal cord preparation from newborn rats. Neurosci Lett 401:194–198.
Schwarzacher SW, Smith JC, Richter DW (1995) Pre-Botzinger complex in the cat. J Neurophysiol 73:1452–1461.
Schwarzacher SW, Pestean A, Gunther S, Ballanyi K (2002) Serotonergic modulation of respiratory motoneurons and interneurons in brainstem slices of perinatal rats. Neuroscience 115:1247–1259.
Shvarev YN, Lagercrantz H, Yamamoto Y (2003) Two types of rhythm in the respiratory network output in the isolated ventrolateral medulla in the neonatal rats. Neurosci Lett 347:53–56.
Smith JC, Ellenberger HH, Ballanyi K, Richter DW, Feldman JL (1991) Pre-Bötzinger complex: a brainstem region that may generate respiratory rhythm in mammals. Science 254:726–729.
Smith JC, Butera RJ, Koshiya N, Del Negro C, Wilson CG, Johnson SM (2000) Respiratory rhythm generation in neonatal and adult mammals: the hybrid pacemaker-network model. Respir Physiol 122:131–147.
Somjen GG (2002) Ion regulation in the brain: implications for pathophysiology. Neuroscientist 8:254–267.
Stosiek C, Garaschuk O, Holthoff K, Konnerth A (2003) In vivo two-photon calcium imaging of neuronal networks. Proc Natl Acad Sci USA 100:7319–7324.
Thoby-Brisson M, Trinh JB, Champagnat J, Fortin G (2005) Emergence of the pre-Botzinger respiratory rhythm generator in the mouse embryo. J Neurosci 25:4307–4318.
Töpert C, Doring F, Wischmeyer E, Karschin C, Brockhaus J, Ballanyi K, Derst C, Karschin A (1998) Kir2.4: a novel K^+ inward rectifier channel associated with motoneurons of cranial nerve nuclei. J Neurosci 18:4096–4105.
Yuste R, Konnerth A, Masters BR (2006) Imaging in neuroscience and development, a laboratory manual. J Biomed Opt 11:19902.